



Published in final edited form as:

*Proteins*. 2012 February ; 80(2): 649–654. doi:10.1002/prot.23147.

## Structural characterization of human Uch37.

E. Sethe Burgie<sup>1</sup>, Craig A. Bingman<sup>1</sup>, Ameet B. Soni<sup>2</sup>, and George N. Phillips Jr.<sup>1,\*</sup>

<sup>1</sup>Department of Biochemistry, Center for Eukaryotic Structural Genomics, University of Wisconsin-Madison, Madison Wisconsin 53706-1544

<sup>2</sup>Department of Computer Sciences, University of Wisconsin-Madison

### Abstract

Uch37 is a de-ubiquitylating enzyme that is functionally linked with the 26S proteasome via Rpn13, and is essential for metazoan development. Here, we report the X-ray crystal structure of full-length human Uch37 at 2.95 Å resolution. Uch37's catalytic domain is similar to those of all UCH enzymes characterized to date. The C-terminal extension is elongated, predominantly helical and contains coiled coil interactions. Additionally, we provide an initial characterization of Uch37's oligomeric state and identify a systematic error in previous analyses of Uch37 activity. Taken together, these data provide a strong foundation for further analysis of Uch37's several functions.

### Keywords

Proteasome; Ubiquitin; Protein assembly; Deubiquitylating enzymes; Ubiquitin C-terminal hydrolase; UCH-L5

### Introduction

Uch37 is a de-ubiquitylating enzyme (DUB) that is functionally linked with multiple protein complexes and signal transduction pathways. Uch37 associates with the 26S proteasome<sup>1</sup> through Rpn13<sup>2</sup> where it serves to remove distal ubiquitin moieties from polyubiquitylated proteins.<sup>1</sup> Uch37's proteasome associated activity was shown to liberate proteins from destruction.<sup>1</sup> However, Uch37 may also specifically facilitate the destruction of inducible nitric oxide synthase and IκB-α at the proteasome.<sup>3</sup> Wicks et al.<sup>4</sup> established Uch37's potential to modulate the transforming growth factor-β(TGF-β) signaling cascade, through its interaction with SMAD7. Yao et al.<sup>5</sup> demonstrated that Uch37 also associates with the Ino80 chromatin-remodeling complex (Ino80 complex), which is involved in DNA repair and transcriptional regulation. Uch37's importance in metazoan development was underscored recently as Uch37 knockouts in mice result in prenatal lethality, where mutant embryos had severe defects in brain development.<sup>6</sup>

\*Correspondence to: Dr. George N. Phillips, Jr., Department of Biochemistry, University of Wisconsin-Madison, 433 Babcock Drive, Madison, WI 53706-1544, Phone: (608) 263-6142, phillips@biochem.wisc.edu.

Protein ubiquitylation is an ATP-dependent post-translational modification that serves to signal a wide variety of cellular processes in eukaryotes.<sup>7,8</sup> A protein cascade, generally comprising three enzymes, functions to activate, transport and specifically transfer ubiquitin to the targeted protein, culminating in an isopeptide linkage between the  $\epsilon$ -amino group of a target protein's lysyl residue and the ubiquitin's terminal carboxylate.<sup>9</sup> Monoubiquitylation plays an important role in histone regulation, endocytosis and viral budding.<sup>10</sup> Further processing of the target protein may be accomplished by ubiquitylation of the protein on a different lysine, or through the formation of polyubiquitin chains,<sup>10</sup> where the best-characterized outcome is destruction of the polyubiquitin-labeled protein in the proteasome.<sup>9</sup>

DUBs catalyze the removal of ubiquitin from proteins. This activity serves to reverse the effects of ubiquitination, permit ubiquitin recycling, or liberate free ubiquitin after translation.<sup>11</sup> Uch37, is a cysteine protease from the ubiquitin C-terminal hydrolase (UCH) family.<sup>7</sup> The catalytic domain of UCH enzymes has a central, six-stranded, antiparallel  $\beta$ -sheet that is flanked on each side by  $\alpha$ -helices.<sup>12</sup> Like picornain 3C, UCH family proteins contain a catalytic triad comprising the side chains of cysteine, histidine, and aspartate. In picornain 3C, the aspartate's carboxylate side chain acts to position histidine's imidazole group for general base catalysis, which activates cysteine for nucleophilic attack.<sup>13</sup> UCH enzymes also contain a glutamine, which may serve to stabilize the tetrahedral transition state.<sup>11</sup> The UCH family can be divided into two distinct groups, i.e., enzymes solely composed of the globular UCH fold, or enzymes comprising the UCH domain and a C-terminal extension. The latter group can be subdivided based on the composition of the C-terminal extension.<sup>14</sup> Uch37 carries a C-terminal extension. Until now the structure of a full-length UCH from this structural class has not been reported.

In this article we report the X-ray crystal structure of full-length human Uch37 at 2.95 Å resolution. This model provides a structural rationale for the accessibility of Uch37's C-terminus for Rpn13 binding. The globular catalytic domain of full-length Uch37 is similar to those of all UCHs characterized to date.<sup>12,15-17</sup> The C-terminal extension is elongated, predominantly helical and as predicted contains coiled coils.<sup>11</sup> Chromatographic analysis of Uch37 demonstrated that Uch37's oligomeric state varies as a function of concentration. Uch37's specific activity is sensitive to Uch37 concentration in the absence of a non-specific binding agent, but nearly constant and an order of magnitude higher in the presence of BSA. These data show that activity assays of isolated Uch37 at low protein concentration suffers from a serious systematic error and suggests that the effects of Uch37 binding proteins on Uch37's activity from previous reports may be misleading. After our Uch37 coordinates were released by the PDB<sup>18</sup>, Nishio et al.<sup>17</sup> reported the structure of the UCH domain of Uch37. The work presented here both verifies and expands upon their findings.

## Materials and Methods

### Expression and purification of Uch37

The Center for Eukaryotic Structural Genomics platform for cloning,<sup>19</sup> protein expression,<sup>20</sup> protein purification,<sup>21</sup> and bioinformatics management<sup>22</sup> was utilized to produce selenomethione labeled Uch37 (isoform 3). Uch37 cDNA was cloned into a pDONR221 plasmid (Invitrogen, Carlsbad, CA), and transferred into the pVP16 expression plasmid

(derived from pQE80, Qiagen, Valencia, CA). Uch37 was expressed in *Escherichia coli* B834 p(RARE2) cells in 2 L of self-inducing media. Cell pastes were sonicated and centrifuged. Uch37 was purified from the supernatant by nickel affinity chromatography. TEV protease was used to cleave the His-maltose-binding protein tag,<sup>23</sup> and Uch37 was purified from the tag and TEV protease by nickel affinity chromatography. Uch37 was exchanged into its final buffer via gel filtration chromatography (0.3 mM tris(2-carboxyethyl)phosphine and 5 mM BisTris, pH 7.0). Uch37 was concentrated to 10 mg\*mL<sup>-1</sup>, flash frozen in liquid nitrogen and stored at 193 K. These processes yielded 12.0 mg of selenomethionine-labeled Uch37.

### Uch37 Crystallization and structure solution

Crystal growth conditions were identified using the 192-condition UW192 screen (CESG, Madison, Wisconsin), and Salt Rx HT and Index HT screens (Hampton Research, Aliso Viejo, California). Sitting drop vapor diffusion screens were assembled with a Mosquito crystallization robot (TTP Labtech, Ltd., Royston, UK). Crystals were grown and monitored in Crystal Farms (Bruker AXS, Inc., Madison, Wisconsin) at 4°C and 20°C. Solutions for crystal optimization were assembled with a Genesis RSP 150 robot (Tecan Group, Ltd., Männedorf, Switzerland) with work lists generated by the Sesame laboratory information management system (University of Wisconsin-Madison). Diffraction quality crystals were grown in hanging drop batch experiments at 4°C. Samples were assembled on siliconized cover slips by mixing 2 µl of Uch37 stock solution with 2 µl of precipitant solution (2.6 M sodium formate and 200 mM Tris, pH 8.5), seeded with crushed Uch37 crystals, and incubated in sealed acrylic batch trays. Crystals grew to dimensions of 200 µm × 200 µm × 200 µm after two weeks. Crystals were transferred to artificial mother liquor (1.3 M sodium formate and 100 mM Tris, pH 8.5), and then to a cryoprotectant solution (1.5 M sodium formate, 100 mM Tris, pH 8.5 and 20% ethylene glycol) through three intermediate solutions. The crystals were flash frozen in a 100 K nitrogen stream.

X-ray diffraction data were collected at the General Medicine and Cancer Institute Collaborative Access Team 23-ID-D Beamline at the Argonne National Laboratory's Advanced Photon Source (Argonne, Illinois). Datasets were collected at the selenium peak and edge wavelengths from a single crystal. The datasets were indexed, integrated and scaled using HKL2000.<sup>24</sup> The selenium substructure was characterized using Phenix.hyss<sup>25</sup> and ShelXD.<sup>26,27</sup> Refinement of the selenium positions with automated density modification was conducted with AutoSharp.<sup>28</sup> A workable preliminary model was produced using the ACMI software package (Version 1.3).<sup>29,30</sup> Manual model building with the program COOT<sup>31</sup> and refinement with Phenix<sup>32</sup> using seven TLS groups were conducted *en route* to generating the final model. Initial TLS groups were determined using TLSMD.<sup>33,34</sup> Model validation was conducted using Molprobity<sup>35</sup> and Procheck.<sup>36</sup> Superposition analyses of Uch37 with homologous proteins were conducted using LSQKAB.<sup>37</sup>

### Analysis of Uch37's oligomeric state

Analytical size exclusion gel chromatography was conducted using a 24 ml Superdex 200 GL column (GE Healthcare, Piscataway, New Jersey) with an Äkta FPLC chromatographic system (GE Healthcare) at 4°C. 25 µl of sample were loaded per run. Protein elution was

monitored by UV-spectroscopy at 280 nm. The elution buffer comprised 200 mM NaCl, 1 mM tris(2-carboxyethyl)phosphine, and 50 mM HEPES, pH 7.5 at 4°C. The column was calibrated with blue dextran, bovine  $\gamma$ -globulin, bovine serum albumin, chicken ovalbumin and equine myoglobin. Buried surface area was calculated using PISA.<sup>38</sup>

### Uch37 reaction kinetics

All kinetic assays were conducted at 25°C, in 200 mM NaCl, 1 mM dithiothreitol, 4% dimethylsulfoxide, 10  $\mu$ M ubiquitin-AMC (Boston Biochem) and 100 mM HEPES, pH 7.5 at 25°C. When included in solution, BSA was added to 2 mg\*ml<sup>-1</sup>. Uch37 was included to 0.25, 1 or 4 nM. Reactions were initiated by the addition of ubiquitin-AMC, and samples were manually mixed. Reaction progress was monitored using a QuantaMaster Model C-60/2000 Spectrofluorimeter (Photon Technologies International, Birmingham, New Jersey) using an excitation wavelength of 380 nM and an emission wavelength of 460 nM.

## Results and Discussion

The structure of Uch37 was solved to a resolution of 2.95 Å. Selenomethionine-labeled Uch37 crystallized in the I222 space group with one polypeptide chain per asymmetric unit. Initial phases were calculated by multiple-wavelength anomalous dispersion (MAD). ACMI<sup>29,30</sup> provided an initial model of Uch37's catalytic domain, and traced the Uch37 C-terminal extension to facilitate model building. Data collection and refinement statistics are listed in Table I.

Uch37 comprises an N-terminal catalytic domain characteristic of the UCH family, and an extended C-terminal extension (Figure 1A). Residues 1-6 and 145-161 of the catalytic domain, and 249-254 and 312-328 of the C-terminal domain were not modeled for lack of interpretable electron density. The presence of the C-terminal extension does not significantly alter the overall fold of the isolated catalytic domain as solved by Nishio et al.<sup>17</sup> Superposition of Uch37 with the ubiquitin-bound form of UCH-L3<sup>16</sup> reveals that the contacts observed between UCH-L3 and ubiquitin can be translated into plausible Uch37-ubiquitin contacts (Figure 1B), and that the crystallographic orientation of the C-terminal domain would not hinder ubiquitin binding.

The C-terminal domain comprises  $\alpha$ -helices 8-10, and a helical segment comprising residues 306-311. The absence of electron density for residues 312 through 328 suggests that this segment, which is essential for Rpn13 binding,<sup>39</sup> may be freely accessible. Helix 8 comprises residues 227 through 245. In a truncation mutant containing the N-terminal 240 amino acids, Helix 8 appears to form spontaneously (Prof. Chittaranjan Das, personal communication). Helix 8 forms a coiled-coil with residues 255 through Glu273 of Helix 9. The coiled coil was predicted previously,<sup>11</sup> and receives its integrity from several hydrophobic interactions throughout its length. Interestingly, within the crystal this coiled coil places Helix 9 in position to interact with bound ubiquitin near ubiquitin's Lys48 (Fig 1C), and could potentially serve to enforce Uch37's selectivity for the distal ubiquitin of polyubiquitin chains.

Uch37 forms a homotetramer with  $D_2$  symmetry within the crystal (Figure 1D). The tetramer assembles as a dimer of dimers. Dimers are formed as Helix 9 from the C-terminal domain of one subunit interacts with the ubiquitin binding face of the catalytic domain from a second subunit, and the C-terminal extensions of the two subunits cross between Helices 9 and 10 for a total buried surface area of  $1861 \text{ \AA}^2$  per subunit. The dimers unite to form a tetramer, primarily through coiled-coil interactions mediated by Helix 10 from each subunit. Each set of contacts at the inter-dimer interface is related by  $D_2$  symmetry to three identical interactions, and have a total buried surface area of  $735 \text{ \AA}^2$  per subunit.

Uch37's weight average molecular weight increases as a function of its concentration. By size-exclusion chromatography, the apparent molecular weight of Uch37 was 51, 56, 70 and 109 kDa at 0.15, 0.69, 2.4 and  $9.5 \text{ mg} \cdot \text{ml}^{-1}$ , respectively. Given Uch37's monomeric molecular weight of 37 kDa and its apparent elongated shape, its tendency toward an apparent molecular weight between 40 and 50 kDa at decreasing concentrations is appropriate for Uch37 monomers. At the highest concentration the molecular weight was increasing sharply as a function of concentration. Thus, the upper limit of Uch37's molecular weight could not be estimated. Uch37 is clearly a self-associating molecule, but under the conditions tested, oligomerization occurs at concentrations that may not be attainable within the cell. However, the crystallographic tetramer is intriguing as it predicts Uch37 auto-inhibition, as Helix 9 would occlude the ubiquitin binding-site. This affords the possibility that under cellular conditions, e.g., through molecular crowding, small molecule association, etc., free Uch37 could reside in an inert form until acted upon by the proteasome, Ino80 complex or other activity modulator.

*In vitro* binding of Uch37 with Rpn13 was shown to promote the hydrolysis of ubiquitin-7-amido-4-methylcoumarin (Ub-AMC) and Uch37's reactivity with suicide inhibitors such as ubiquitin vinylsulfone (UbVS) and ubiquitin aldehyde (Ubal).<sup>2</sup> Activation appeared to be regulated in part by the C-terminal domain of Uch37,<sup>2</sup> as removal of the residues 238-329 provided enhanced hydrolase activity. However, this modification did not restore the same degree of activity that was achieved by the Rpn13-Uch37 complex.<sup>2</sup> An alternative explanation for these phenomena is the differential solubility of Uch37 at low concentrations. To test this possibility we conducted assays of Uch37 to approximate concentrations and conditions previously assayed<sup>2,5</sup> with or without bovine serum albumin (BSA) as a non-specific binding agent (Figure 1E). In the absence of BSA, Uch37 specific activity was relatively low, and was highly dependent upon the Uch37 concentration. At increasing Uch37 concentrations Uch37 specific activity increased dramatically. Two processes could explain this, oligomerization of Uch37 yielding a more active form, or a disproportionate loss of functional Uch37 through nonspecific binding. However, in the presence of BSA, Uch37 specific activity was one to two orders of magnitude higher than it was in the absence of BSA and constant as a function of concentration, suggesting the latter mechanism. Thus, additives that could stabilize Uch37 solubility through a direct binding event, e.g., Rpn13, or chemical modifications of Uch37 that may yield a more soluble form, e.g., removal of the C-terminal tail could enhance Uch37's activity. These observations do not preclude the possibility that Rpn13 enhances Uch37 activity. However, they do show the presence of a serious systematic error in prior investigations that could lead to incorrect assumptions of Uch37's activity.

In conclusion, Uch37 consists of two domains, a globular UCH-domain and a fibrous C-terminal tail. The C-terminal residues of Uch37 implicated in Rpn13 binding appear to be unstructured and solvent exposed. Uch37 undergoes a dynamic equilibrium between monomers and higher order oligomers. Within the crystal, Uch37 is tetrameric with subunit contacts that would preclude ubiquitin binding. However, the concentrations required for oligomerization are high and would be unlikely to provide significant inhibition against Uch37's activity unless cellular conditions promoted self-assembly. The rates of ubiquitin-AMC hydrolysis by Uch37 are much higher in the presence of the non-specific binding agent, BSA, than in its absence. This result reveals a systematic error in similar assays that have been used to characterize the effects of mutations and Uch37 binding proteins on Uch37 activity and function. Finally, our Uch37 structure provides a suitable molecular model for probing the interactions of Uch37 with its various partner molecules.

## Acknowledgments

This work was supported by the National Library of Medicine training grant T15-LM007359, NLM R01-LM008796, and NIH Protein Structure Initiative Grant GM074901. We gratefully acknowledge all members of the Center for Eukaryotic Structural Genomics. We would like to thank Chris Bianchetti and Aram Chang for reviewing portions of the manuscript. We thank LS-CAT Sector 21 for use of their facilities in the initial screening phase of our research efforts. Use of LS-CAT Sector 21 was supported by the Michigan Economic Development Corporation and the Michigan Technology Tri-Corridor (Grant 085P1000817). We laud the GM/CA CAT staff for facilitating collection of the final data sets. GM/CA CAT has been funded in whole or in part with Federal funds from the National Cancer Institute (Y1-CO-1020) and the National Institute of General Medical Science (Y1-GM-1104). Use of the Advanced Photon Source was supported by the U.S. Department of Energy, Basic Energy Sciences, Office of Science, under contract No. DE-AC02-06CH11357. Fluorescence data were obtained at the University of Wisconsin-Madison Biophysics Instrumentation Facility (BIF), which was established with support from the University of Wisconsin-Madison and grants BIR-9512577 (NSF) and S10 RR13790 (NIH). We also thank the BIF facilities manager, Dr. Darrell R. McCaslin, for helpful discussions

## References

1. Lam YA, Xu W, DeMartino GN, Cohen RE. Editing of ubiquitin conjugates by an isopeptidase in the 26S proteasome. *Nature*. 1997; 385(6618):737–740. [PubMed: 9034192]
2. Yao T, Song L, Xu W, DeMartino GN, Florens L, Swanson SK, Washburn MP, Conaway RC, Conaway JW, Cohen RE. Proteasome recruitment and activation of the Uch37 deubiquitinating enzyme by Adrm1. *Nat Cell Biol*. 2006; 8(9):994–1002. [PubMed: 16906146]
3. Mazumdar T, Gorgun FM, Sha Y, Tyryshkin A, Zeng S, Hartmann-Petersen R, Jorgensen JP, Hendil KB, Eissa NT. Regulation of NF-kappaB activity and inducible nitric oxide synthase by regulatory particle non-ATPase subunit 13 (Rpn13). *Proc Natl Acad Sci U S A*. 2010; 107(31):13854–13859. [PubMed: 20634424]
4. Wicks SJ, Haros K, Maillard M, Song L, Cohen RE, Dijke PT, Chantry A. The deubiquitinating enzyme UCH37 interacts with Smads and regulates TGF-beta signalling. *Oncogene*. 2005; 24(54):8080–8084. [PubMed: 16027725]
5. Yao T, Song L, Jin J, Cai Y, Takahashi H, Swanson SK, Washburn MP, Florens L, Conaway RC, Cohen RE, Conaway JW. Distinct modes of regulation of the Uch37 deubiquitinating enzyme in the proteasome and in the Ino80 chromatin-remodeling complex. *Mol Cell*. 2008; 31(6):909–917. [PubMed: 18922472]
6. Al-Shami A, Jhaveri KG, Vogel P, Wilkins C, Humphries J, Davis JJ, Xu N, Potter DG, Gerhardt B, Mullinax R, Shirley CR, Anderson SJ, Oravec T. Regulators of the proteasome pathway, Uch37 and Rpn13, play distinct roles in mouse development. *PLoS One*. 2010; 5(10):e13654. [PubMed: 21048919]
7. Ciechanover A. The ubiquitin-proteasome proteolytic pathway. *Cell*. 1994; 79(1):13–21. [PubMed: 7923371]

8. Weake VM, Workman JL. Histone ubiquitination: triggering gene activity. *Mol Cell*. 2008; 29(6): 653–663. [PubMed: 18374642]
9. Hershko A, Ciechanover A. The ubiquitin system. *Annu Rev Biochem*. 1998; 67:425–479. [PubMed: 9759494]
10. Ventii KH, Wilkinson KD. Protein partners of deubiquitinating enzymes. *Biochem J*. 2008; 414(2): 161–175. [PubMed: 18687060]
11. Komander D, Clague MJ, Urbe S. Breaking the chains: structure and function of the deubiquitinases. *Nat Rev Mol Cell Biol*. 2009; 10(8):550–563. [PubMed: 19626045]
12. Johnston SC, Larsen CN, Cook WJ, Wilkinson KD, Hill CP. Crystal structure of a deubiquitinating enzyme (human UCH-L3) at 1.8 Å resolution. *EMBO J*. 1997; 16(13):3787–3796. [PubMed: 9233788]
13. Sarkany Z, Polgar L. The unusual catalytic triad of poliovirus protease 3C. *Biochemistry*. 2003; 42(2):516–522. [PubMed: 12525179]
14. Yang P, Smalle J, Lee S, Yan N, Emborg TJ, Vierstra RD. Ubiquitin C-terminal hydrolases 1 and 2 affect shoot architecture in *Arabidopsis*. *Plant J*. 2007; 51(3):441–457. [PubMed: 17559514]
15. Johnston SC, Riddle SM, Cohen RE, Hill CP. Structural basis for the specificity of ubiquitin C-terminal hydrolases. *EMBO J*. 1999; 18(14):3877–3887. [PubMed: 10406793]
16. Misaghi S, Galardy PJ, Meester WJ, Ovaa H, Ploegh HL, Gaudet R. Structure of the ubiquitin hydrolase UCH-L3 complexed with a suicide substrate. *J Biol Chem*. 2005; 280(2):1512–1520. [PubMed: 15531586]
17. Nishio K, Kim SW, Kawai K, Mizushima T, Yamane T, Hamazaki J, Murata S, Tanaka K, Morimoto Y. Crystal structure of the de-ubiquitinating enzyme UCH37 (human UCH-L5) catalytic domain. *Biochem Biophys Res Commun*. 2009; 390(3):855–860. [PubMed: 19836345]
18. Berman HM, Westbrook J, Feng Z, Gilliland G, Bhat TN, Weissig H, Shindyalov IN, Bourne PE. The Protein Data Bank. *Nucleic Acids Res*. 2000; 28(1):235–242. [PubMed: 10592235]
19. Thao S, Zhao Q, Kimball T, Steffen E, Blommel PG, Ritters M, Newman CS, Fox BG, Wrobel RL. Results from high-throughput DNA cloning of *Arabidopsis thaliana* target genes using site-specific recombination. *J Struct Funct Genomics*. 2004; 5(4):267–276. [PubMed: 15750721]
20. Sreenath HK, Bingman CA, Buchan BW, Seder KD, Burns BT, Geetha HV, Jeon WB, Vojtik FC, Aceti DJ, Frederick RO, Phillips GN Jr. Fox BG. Protocols for production of selenomethionine-labeled proteins in 2-L polyethylene terephthalate bottles using auto-induction medium. *Protein Expr Purif*. 2005; 40(2):256–267. [PubMed: 15766867]
21. Jeon WB, Aceti DJ, Bingman CA, Vojtik FC, Olson AC, Ellefson JM, McCombs JE, Sreenath HK, Blommel PG, Seder KD, Burns BT, Geetha HV, Harms AC, Sabat G, Sussman MR, Fox BG, Phillips GN Jr. High-throughput purification and quality assurance of *Arabidopsis thaliana* proteins for eukaryotic structural genomics. *J Struct Funct Genomics*. 2005; 6(2-3):143–147. [PubMed: 16211511]
22. Zolnai Z, Lee PT, Li J, Chapman MR, Newman CS, Phillips GN Jr. Rayment I, Ulrich EL, Volkman BF, Markley JL. Project management system for structural and functional proteomics: Sesame. *J Struct Funct Genomics*. 2003; 4(1):11–23. [PubMed: 12943363]
23. Blommel PG, Fox BG. A combined approach to improving large-scale production of tobacco etch virus protease. *Protein Expr Purif*. 2007; 55(1):53–68. [PubMed: 17543538]
24. Otwinowski Z, Minor W. Processing of X-ray diffraction data collected in oscillation mode. *Method Enzymol*. 1997; 276:307–326.
25. Grosse-Kunstleve RW, Adams PD. Substructure search procedures for macromolecular structures. *Acta Crystallogr D Biol Crystallogr*. 2003; 59(Pt 11):1966–1973. [PubMed: 14573951]
26. Schneider TR, Sheldrick GM. Substructure solution with SHELXD. *Acta Crystallogr D Biol Crystallogr*. 2002; 58(Pt 10 Pt 2):1772–1779. [PubMed: 12351820]
27. Uson I, Sheldrick GM. Advances in direct methods for protein crystallography. *Curr Opin Struct Biol*. 1999; 9(5):643–648. [PubMed: 10508770]
28. Vonrhein C, Blanc E, Roversi P, Bricogne G. Automated structure solution with autoSHARP. *Methods Mol Biol*. 2007; 364:215–230. [PubMed: 17172768]

29. DiMaio F, Kondrashov DA, Bitto E, Soni A, Bingman CA, Phillips GN Jr, Shavlik JW. Creating protein models from electron-density maps using particle-filtering methods. *Bioinformatics*. 2007; 23(21):2851–2858. [PubMed: 17933855]
30. DiMaio F, Shavlik J, Phillips GN. A probabilistic approach to protein backbone tracing in electron density maps. *Bioinformatics*. 2006; 22(14):e81–89. [PubMed: 16873525]
31. Emsley P, Cowtan K. Coot: model-building tools for molecular graphics. *Acta Crystallogr D Biol Crystallogr*. 2004; 60(Pt 12 Pt 1):2126–2132. [PubMed: 15572765]
32. Afonine PV, Grosse-Kunsteve RW, Adams PD. The Phenix refinement framework. *CCP4 Newsl*. 2005; 42 contribution 8.
33. Painter J, Merritt EA. Optimal description of a protein structure in terms of multiple groups undergoing TLS motion. *Acta Crystallogr D Biol Crystallogr*. 2006; 62(Pt 4):439–450. [PubMed: 16552146]
34. Painter J, Merritt EA. TLSMD web server for the generation of multi-group TLS models. *Journal of Applied Crystallography*. 2006; 39:109–111.
35. Davis IW, Leaver-Fay A, Chen VB, Block JN, Kapral GJ, Wang X, Murray LW, Arendall WB 3rd, Snoeyink J, Richardson JS, Richardson DC. MolProbity: all-atom contacts and structure validation for proteins and nucleic acids. *Nucleic Acids Res*. 2007; 35(Web Server issue):W375–383. [PubMed: 17452350]
36. Laskowski RA, MacArthur MW, Moss DS, Thornton JM. Procheck - a Program to Check the Stereochemical Quality of Protein Structures. *Journal of Applied Crystallography*. 1993; 26:283–291.
37. Kabsch W. Solution for Best Rotation to Relate 2 Sets of Vectors. *Acta Crystallographica Section A*. 1976; 32(Sep1):922–923.
38. Krissinel E, Henrick K. Inference of macromolecular assemblies from crystalline state. *J Mol Biol*. 2007; 372(3):774–797. [PubMed: 17681537]
39. Hamazaki J, Iemura S, Natsume T, Yashiroda H, Tanaka K, Murata S. A novel proteasome interacting protein recruits the deubiquitinating enzyme UCH37 to 26S proteasomes. *EMBO J*. 2006; 25(19):4524–4536. [PubMed: 16990800]

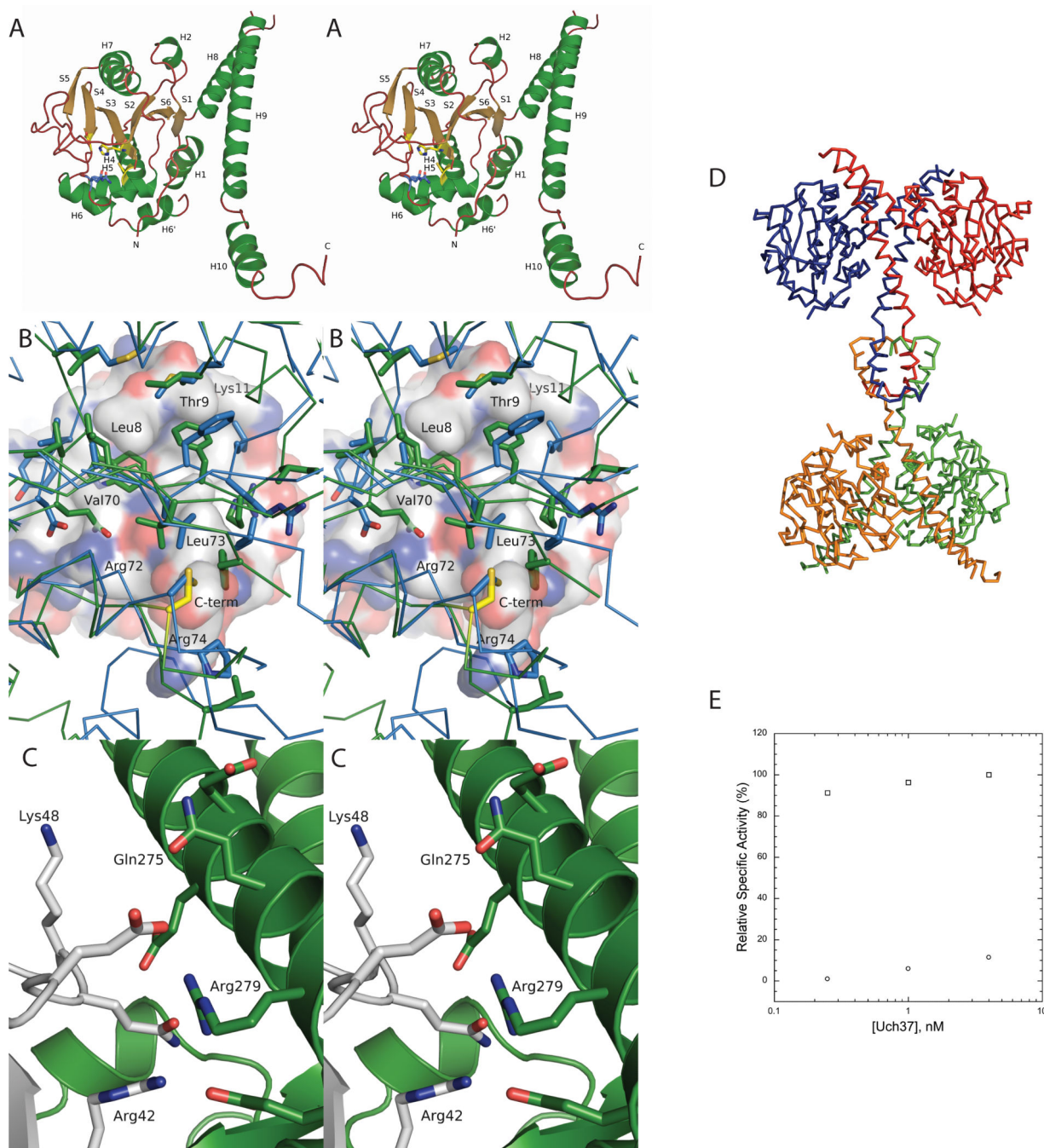


**Figure 1. Uch37 structure and activity**

**(A)** Uch37 is rendered as a cartoon stereodiagram.  $\alpha$ -helices are labeled H1-H10, and  $\beta$ -strands are labeled S1-S6. Catalytic triad residues (Cys88, His 164 and Asp179) are rendered as sticks and highlighted with yellow, and Gln82, which is putatively involved in transition state stabilization is highlighted in blue. **(B)** The superposition of Uch37 (green) with ubiquitin-bound UCH-L3<sup>16</sup> (blue) is illustrated as a stereodiagram. Ubiquitin is displayed as a surface where carbon, oxygen and nitrogen atoms are colored white, red and blue, respectively. Positions of ubiquitin residues are labeled for convenience. The Uch37

catalytic cysteine is highlighted in yellow. **(C)** The relative position of Uch37's (green) Helix 9 and the superposed ubiquitin (white) from the UCH-L3-ubiquitin complex is displayed as a stereodiagram. **(D)** The crystallographic Uch37 tetramer is shown as a ribbon diagram. Subunits are distinguished by color. **(E)** The relative specific activity of Uch37 in the presence (□) or absence (○) of BSA are plotted as a function of Uch37 concentration.

**Table I**

## Crystal Parameters, Xray Data Collection, and Refinement Statistics

	Peak	Inflection
Crystal parameters		
Space group	I222	I222
Unit-cell parameters (Å)	90.0 × 98.7 × 154.0	90.1 × 98.7 × 154.0
Data collection statistics <sup>a</sup>		
Wavelength (Å)	0.97949	0.97973
Resolution range (Å)	50-2.95(3.10-2.95)	50-2.95(3.10-2.95)
No. of reflections	13687(1252)	13648(1243)
Completeness (%)	93.3(69.1)	92.8(68.3)
$R_{merge}$ <sup>b</sup>	0.074(0.278)	0.057(0.292)
Redundancy	11.7(10.3)	11.7(10.0)
$\langle I \rangle / \sigma(I)$	36.4(7.0)	36.9(6.1)
Refinement and model statistics <sup>a</sup>		
Resolution range (Å)	45.6-2.95(3.18-2.95)	
No. of reflections (work/test)	13114/682	
Completeness (%)	92.9(71)	
$R_{cryst}$ <sup>c</sup>	0.201(0.248)	
$R_{free}$ <sup>d</sup>	0.242(0.278)	
RMSD bonds (Å)	0.007	
RMSD angles (°)	1.09	
B factor- overall/protein/waters (Å)	107.2/107.1/70.0	
No. of protein molecules/all atoms <sup>e</sup>	1/2290	
Ramachandran plot by MOLPROBITY (%)		
Favored region	92.4	
Additionally allowed region	7.6	
Outliers	0	
PDB code	3IHR	

<sup>a</sup>Values in parentheses are for the highest resolution shell.

<sup>b</sup> $R_{merge} = \frac{\sum_h \sum_i |I_i(h) - \langle I(h) \rangle|}{\sum_h \sum_i I_i(h)}$ , where  $I_i(h)$  is the intensity of an individual measurement of the reflection and  $\langle I(h) \rangle$  is the mean intensity of the reflection.

<sup>c</sup> $R_{cryst} = \frac{\sum_h ||F_{obs}| - |F_{calc}||}{\sum_h |F_{obs}|}$ , where  $F_{obs}$  and  $F_{calc}$  are the observed and calculated structure-factor amplitudes, respectively.

<sup>d</sup> $R_{free}$  was calculated as  $R_{cryst}$  using the randomly selected unique reflections (~5%) that were omitted from structural refinement.

<sup>e</sup>These include atoms from 10 water molecules, 2 formate ions, and one sodium ion.